



Supplementary Materials for

Mixed-Phase Oxide Catalyst Based on Mn-Mullite (Sm, Gd)Mn₂O₅ for NO Oxidation in Diesel Exhaust

Weichao Wang,* Geoffrey McCool, Neeti Kapur, Guang Yuan, Bin Shan, Matt Nguyen,
Uschi M. Graham, Burtron H. Davis, Gary Jacobs, Kyeongjae Cho,* Xianghong (Kelly)
Hao*

*To whom correspondence should be addressed. E-mail: wwang@nanostellar.com (W.W.);
kjcho@utdallas.edu (K.C.); xhao@nanostellar.com (X.H.)

Published 17 August 2012, *Science* **337**, 832 (2012)
DOI: 10.1126/science.1225091

This PDF file includes:

Materials and Methods (S-I to S-VII)
Supplementary Text (S-VIII to S-X)
Figs. S1 to S6
Tables S1 to S3
References (15–19)

Materials and Methods

S-I. Preparation of Mixed-Phase Oxides and Pt Reference Catalyst

Mixed metal oxide catalysts were prepared by a co-precipitation method. Appropriate amounts of $\text{Mn}(\text{CH}_3\text{CO}_2)_2 \cdot 4\text{H}_2\text{O}$, $\text{Sr}(\text{NO}_3)_2$, $\text{Ce}(\text{NO}_3)_3 \cdot 6\text{H}_2\text{O}$, $\text{Sm}(\text{NO}_3)_3 \cdot 6\text{H}_2\text{O}$, $\text{Gd}(\text{NO}_3)_3 \cdot 6\text{H}_2\text{O}$ (all metal salt precursors are from Alfa-Aesar), and Pluronic F127 (Sigma-Aldrich) were dissolved in deionized water, with adequate stirring. Alternately, $\text{Mn}(\text{NO}_3)_2$, MnCO_3 , $\text{Ce}_2(\text{CO}_3)_3$ or Sm_2O_3 (the last three were dissolved in nitric acid) can be used as precursors and PEG-600 can be used as a co-surfactant. A 25% solution of tetramethylammonium hydroxide (TMAH, from Sachem) was then added to increase the pH to 9-10. Oxalic acid (10% excess with regard to Sr) dissolved in TMAH was added, followed by the drop-wise addition of 30-35% hydrogen peroxide (H_2O_2) (20-50% excess with regard to Mn and Ce) utilizing octanol as a defoaming agent as needed. More TMAH or 29% ammonium hydroxide ($\text{NH}_4\text{OH}_{(\text{aq})}$) was added simultaneously along with the H_2O_2 to maintain the pH above 9. Then the mixture stirred for two hours, the precipitate was filtered, dried at 100-110°C overnight, processed with a mortar and pestle, and calcined for 8 hours at 500°C followed by a second calcination step at 8 hours at 800°C in static air. SmMn_2O_5 , strontium manganese oxides, manganese oxide and ceria, were prepared by the same method. 2 wt% Pt on $\gamma\text{-Al}_2\text{O}_3$ (Sasol TH100/150) was prepared by the incipient wetness method using $\text{Pt}(\text{NO}_3)_2$ (Heraeus), calcined for 2 hours at 500°C and hydrothermally aged. The hydrothermal aging conditions for all samples were 10h at 820°C in 10% steam before the NO performance test.

S-II. Catalyst Evaluation Conditions and BET Surface Area Measurement

The sample was prepared by compressing the powder into a pellet, crushing the pellet, and sieving the crushed sample to 80-100 mesh. 10 mg of the sieved sample was diluted with 90 mg of α -alumina (100 mesh) and put into a quartz tube with packed quartz wool to keep it in place.

The sample tube was then placed into a reactor furnace (Altamira Catalyst Characterization System, AMI-200) and flushed continuously with 450 ppm NO and 10% O_2 in He, at a total flow rate of 200 sccm. The furnace was ramped at 10°C/min to 350°C, cooled to ~50°C, and then ramped to 350°C a second time. The NO and NO_2 concentrations were recorded with a NO_x analyzer (EcoPhysics, CLD822CMh) for the first ramp-up and ramp-down cycle.

Fig. S2 reveals that ceria showed no activity while the strontium manganese oxide and manganese oxide displayed a maximum conversion of 30%.

BET surface area measurements were conducted on a Quantachrome Instruments, Autosorb-1 instrument. The sample, ~0.25 g, was placed in a 9 mm bulb tube and degassed for two hours at 300°C. Multipoint BET measurements were conducted using nitrogen gas as an adsorbate at 77 K in the relative pressure range of 0.05-0.35.

S-III. X-Ray Diffraction (XRD) Methods

The catalyst sample was placed on a zero background holder and transferred into a Panalytical X'pert MPD PRO Diffractometer, which employs Cu radiation at

45KV/40mA. Scans were run over the range of 10° to 100° with a step size of 0.0157° and a counting time of 750 seconds per step.

The crystal information of Sr-based manganese oxides ($\text{Sr}_{1.03}\text{MnO}_{2.82}$), mullite (SmMn_2O_5), manganese oxides (MnO_x) and ceria (CeO_2) are shown in Fig. S1. XRD results revealed the mullite phase for Sm-manganese oxide, while Sr-based manganese oxide is predominantly the perovskite phase. Mn oxides are mainly cubic bixbyite structure (Mn_2O_3) with a minor contribution from the Mn_3O_4 spinel phase.

S-IV. Determination of Crystallite Orientations and Composition by Electron Microscopy and EDS

The morphologies of the MnCe-7:1 were observed by field-emission scanning electron microscopy (FESEM FEI Sirion 200) equipped with an energy dispersion X-ray spectrometer (EDS), operated at an acceleration voltage of 10.0 kV, and their chemical compositions were determined by EDS. The resolution is 1.5nm at a specific voltage of 10 kV. Magnification is up to 50000 times. The work distance between camera lens and sample is 5.8 mm.

Nanoparticle morphologies, crystalline structure and local nano- and microstructures were observed in a field emission JEOL 2010 F analytic transmission electron microscope and scanning tunneling electron microscopy (STEM) at an accelerating voltage of 200 kV and a 0.2 nm point resolution. The TEM was equipped with a GATAN 2000 GIF, GATAN DigiScanII, Fischione HAADF STEM detector, Oxford EDS detector and EmiSpec EsVision software.

Additional high resolution TEM images of catalyst MnCe-7:1 are shown in Fig. S3 (A) and (B). Lattice fringes measured in HRTEM images in our experiments correspond to a d-spacing range varying from 5.81 to 5.87 Å, based on a sample size of six crystallites. Pearson's Crystal Data (15) reports a d-spacing of 5.62 Å and 5.69 Å for SmMn_2O_5 (110) and (001) orientations respectively. Hence, both these surface facets are likely to be exposed on MnCe-7:1.

S-V. DRIFTS Experimental Conditions

Diffuse Reflectance Infrared Fourier Transform Spectroscopy (DRIFTS) accessory (Harrick's Praying Mantis) in conjunction with the FTIR (Thermo Nicolet 6700) at 4 cm^{-1} resolution was performed to identify NO wavenumbers for adsorption and oxidation reactions. All data in the experimental sequence was collected every 5 seconds and a total flow rate of 200 sccm of the gas mixture was used in all steps. To maximize the signal of NO related surface species, we chose 1% NO as the concentration for this particular experiment. The experimental sequence was implemented as followed. The catalyst was first pretreated at 400°C with 10% O_2 and then cooled down to 200°C . The reaction chamber was flushed with He for 30 minutes to remove any residue and 50 scans were collected as the background. Thereafter, 1% NO was introduced for 10 minutes. The reaction chamber was once again flushed with He for 30 minutes. 1% NO and 1% O_2 were subsequently introduced for 10 minutes as the last step.

S-VI. DFT Calculations and Surface Model Details

Gradient-corrected density functional theory (DFT) calculations (16) were carried out using plane waves as implemented in Vienna Ab initio Simulation Package (VASP). The Kohn-Sham single electron orbitals were expanded by plane waves with an energy cutoff of 400 eV. The geometry optimization is considered complete when the Hellmann-Feynman force on each atom is less than 0.02 eV/Å. Transition states were obtained by performing nudged elastic band (NEB) calculations (17), which assists in finding the saddle points between two local minima for the system.

DFT calculations were performed to examine the detailed NO oxidation mechanism on the SmMn₂O₅ (110) surface. A periodic slab model was generated with a theoretically calculated lattice constant of 5.84 Å, which is in agreement with the experimental value of 5.69 Å (18). A total of 98 atoms were included in the slab model with a thickness of eight atomic layers, such that the bottom two atomic layers were fixed at their bulk positions. A vacuum layer of 10 Å was added to avoid intermolecular interactions. A 4×4×1 k-point mesh was used for Brillouin zone integration.

Mullite oxides (Sm, Gd)Mn₂O₅ have an orthorhombic structure (space group pbam) in which Mn³⁺ and Mn⁴⁺ occupy different crystallographic positions in square pyramidal and octahedral coordination environments, respectively (Fig. S3(C)). Atomistic models for SmMn₂O₅ (001) (Fig. S3(D)) and (110) facets (Fig. 2F in main text) were generated based on lattice parameters and symmetry reported in Pearson's Crystal Database. Ideal (001) and (110) surfaces are oxidized and catalytically inert to NO oxidation due to weak adsorption properties. Stepped facets on the other hand (Fig. 2F in the main text for surface (110), Fig. S3(F) for surface (001)), include Mn-Mn dimer atoms which allow spontaneous O₂ dissociation to atomic oxygen. Therefore, Mn-Mn dimer sites are the prerequisite for the NO oxidation reaction to proceed on either of these surface facets. We have discussed the detailed catalytic mechanism for NO oxidation on SmMn₂O₅ (110) stepped surface in the main text.

(S-VII) Simulated Diesel Exhaust Core Test: Preparation and Test Conditions

All of the catalyst samples were coated on cordierite honeycomb substrate with 400 cells/in² and a cell wall thickness of 4 mils; the bottom layer contains a mixture of either 3% Pt-1.5%Pd/γ-Al₂O₃ (Pt:Pd=2:1 wt:wt) or 2.4% Pt-1.6%Pd/γ-Al₂O₃ (Pt:Pd=3:2 wt:wt) and 0.45 g/in³ of zeolite (beta-zeolite: ZSM-5=2:1 wt:wt, Zeolyst CP7119 and CBV2314). The PtPd/ γ-Al₂O₃ (TH100/150 Sasol) powders were prepared as per patent US2009214396. On the DOC catalyst samples with two layers, the top layer was coated with 1 g/in³ of MnCe-7:1. Sample ID and formulations are listed in the table as shown in Table S3.

All of the coated samples were cut into φ 0.5" x 1" cores, and hydrothermally aged at 750°C for 16 hours in air with 10% steam. The aged cores were tested in a bench scale reactor for two cycles, where the exhaust gas was continuously monitored by FT-IR (MKS Multigas 2030). The reaction gas composition used was 1000 ppmv CO, 105 ppmv C₃H₈, 245 ppmv C₃H₆, 100 ppmv *n*-decane, 150 ppmv NO, 10 v/v% O₂, 7 v/v% H₂O and 5 v/v% CO₂, with the gas hourly space velocity (GHSV) of 60,000 h⁻¹. In the first cycle, the furnace temperature ramped up to 400°C at a rate of 10°C/min, and then

cooled down in the reaction gas mixture to 50°C. In the second cycle, the same conditions were repeated. The comparison of the ramp-up test results are discussed in (S-X).

Supplementary Text

S-VIII. DFT Calculated Wavenumbers on Mullite (110) Surface

We correlated the experimental IR bands to potential NO_x surface species by calculating DFT based wavenumbers on oxidized and stepped SmMn₂O₅(110) surfaces as shown in Table SII.

S-IX. O₂ Adsorption and Dissociation and Atomic O* Diffusion on Mn-Mn Sites

Based on the HRTEM image of the (110) facet (Fig. S3(A)), the majority of Sm and Mn atoms are oxidized by O. Thus, these oxidized atoms are inert to further oxidation or NO adsorption. As a result, the oxidized surface might not be responsible for the catalytic activity. A different scenario is observed on a stepped (110) surface on which O₂ readily adsorbs on a Mn-Mn dimer site and subsequently dissociates into atomic O*. Using the NEB method, an O₂ molecule is initially positioned approximately 9 Å away from the stepped (110) surface to the calculated energy barrier of the O₂ dissociating onto the Mn-Mn site. The calculations show that O₂ spontaneously dissociates on the surface and forms atomic O*, which binds to Mn sites. This reveals that Mn-Mn might be the active site for further catalytic reactions.

In order to evaluate atomic O* diffusion on the Mn-Mn dimer, seven intermediate images were inserted linearly between two states, i.e., atop O* atoms positioned on Mn atoms of Mn-Mn dimers. As shown in Fig. S5, as O* approaches the middle of the dimer, the energy gradually decreases by ~0.68 eV. After the midpoint, an energy barrier of 0.55 eV must be overcome for O* to diffuse to another Mn-atop site. The overall results demonstrate that O* has a strong diffusion capability on the Mn-dimer.

S-X. Core Test Performance Results

From the core test results (Fig. S6 (A)-(D)), it can be seen that the MnCe-7:1 layer is not detrimental to CO, C₃H₆ and *n*-decane light-off. The NO₂ yield is increased for the catalysts with a top layer coated with MnCe-7:1.

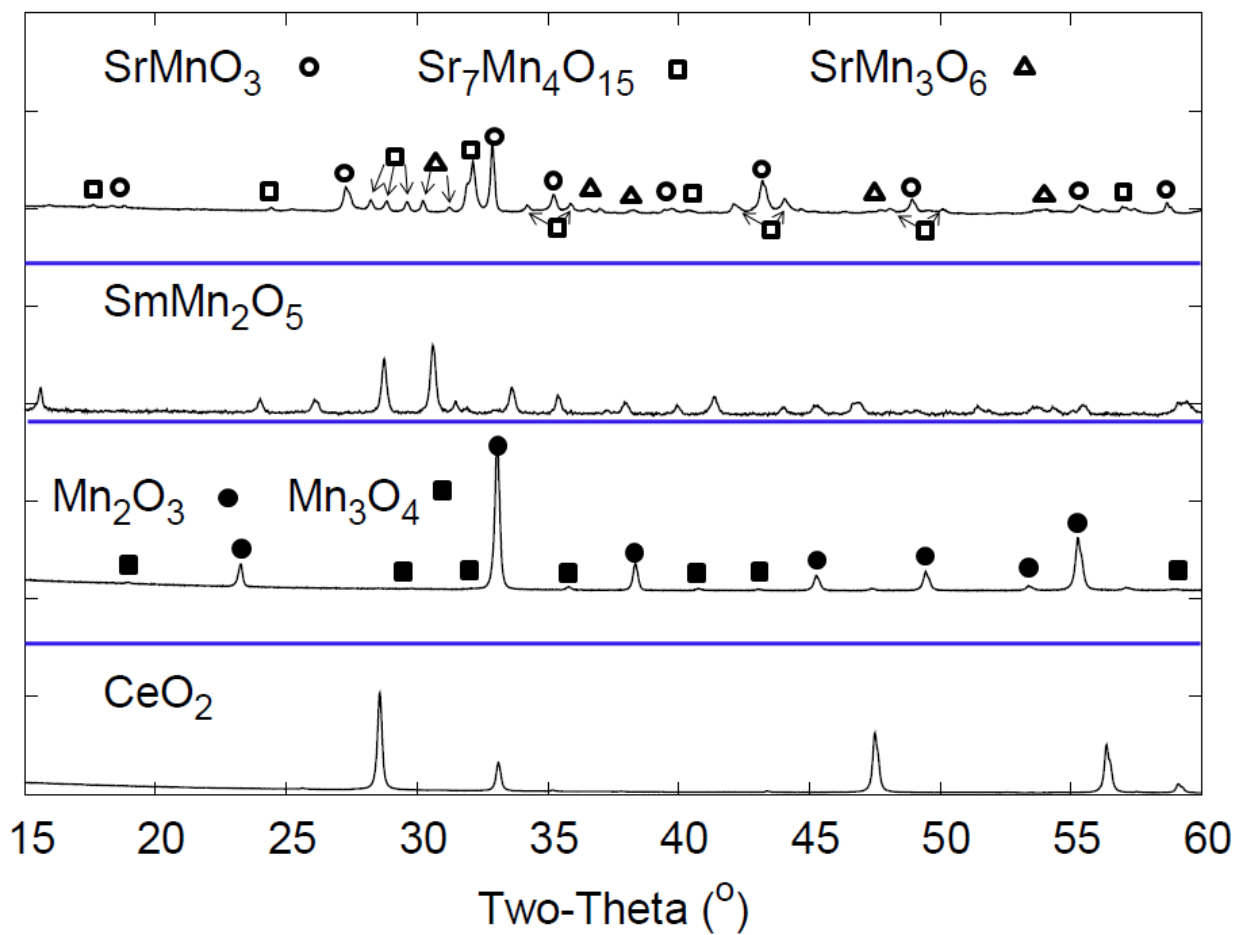


Fig. S1.

XRD pattern of the Sr-manganese oxide ($\text{Sr}_{1.03}\text{MnO}_{2.82}$), Sm-manganese oxide (SmMn_2O_5), manganese oxide (MnO_x) and ceria (CeO_2).

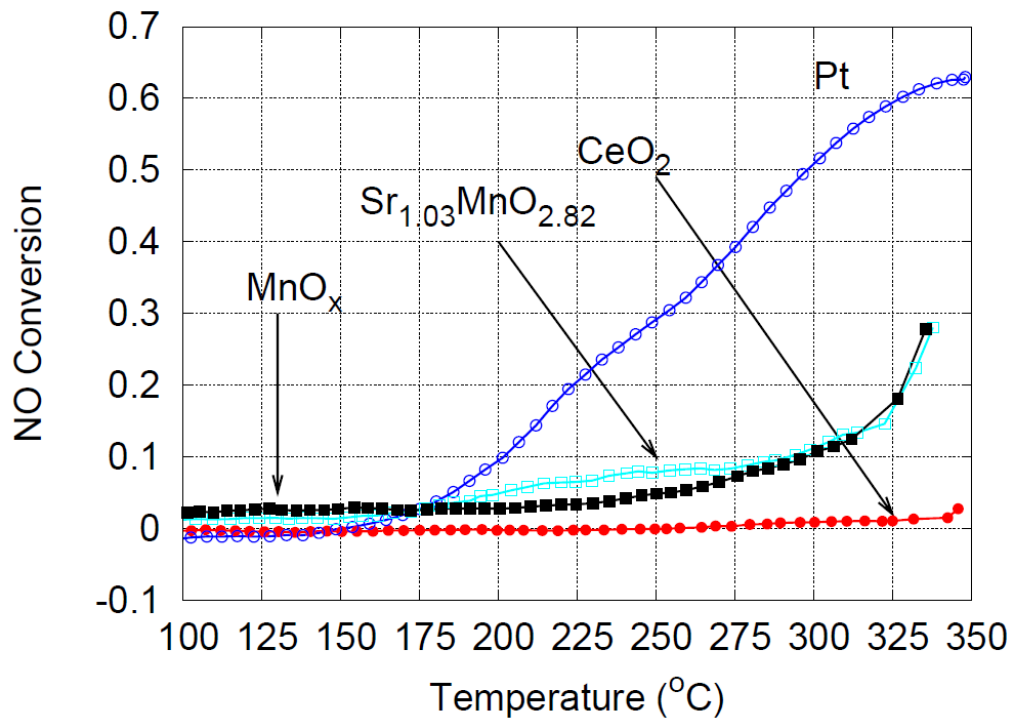
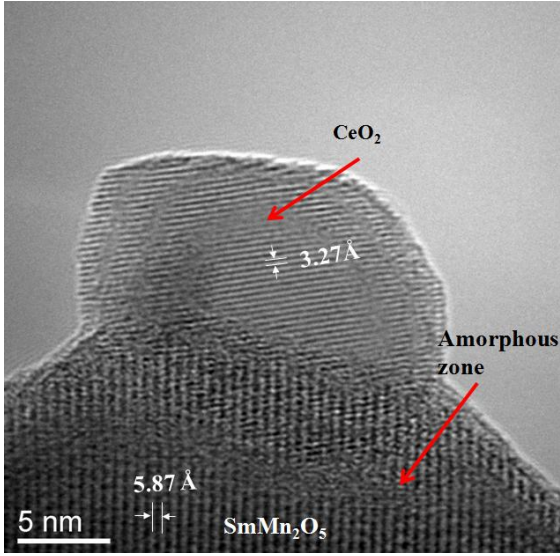
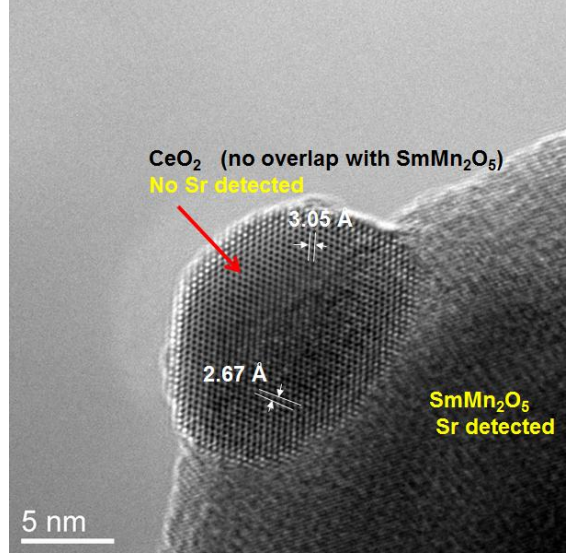


Fig. S2.

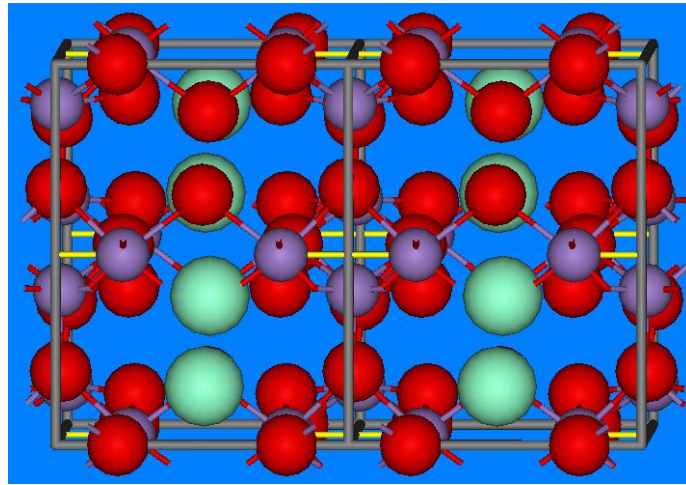
NO conversion versus temperature for manganese oxide (■), strontium manganese oxide (□), CeO₂ (●), and Pt (○).



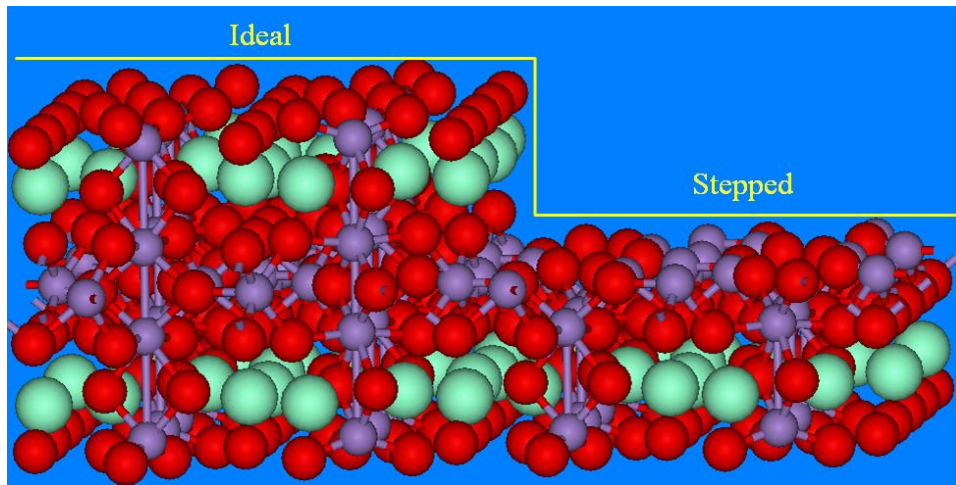
A



B



C



D

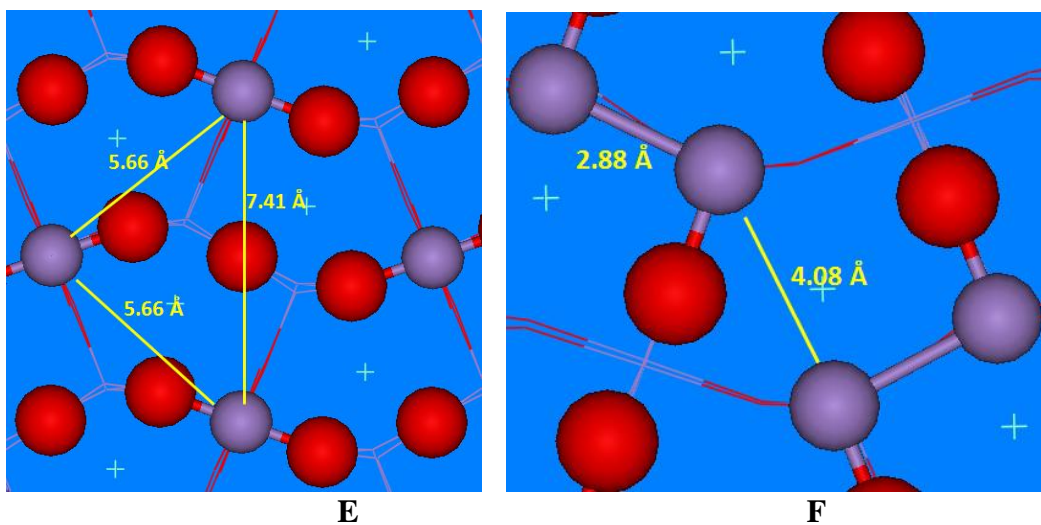


Fig. S3.

(A) and (B) high resolution TEM images of catalyst MnCe-7:1 in different regions; (C) side view of two unit cells of SmMn_2O_5 , Mn-Mn dimers bonds are highlighted as yellow horizontal bars; (D) side view of SmMn_2O_5 (100) ideal and stepped surface. (E) and (F) atomistic models for ideal and stepped (001) surfaces, respectively. Red, purple and light green balls represent O, Mn, and Sm, respectively.

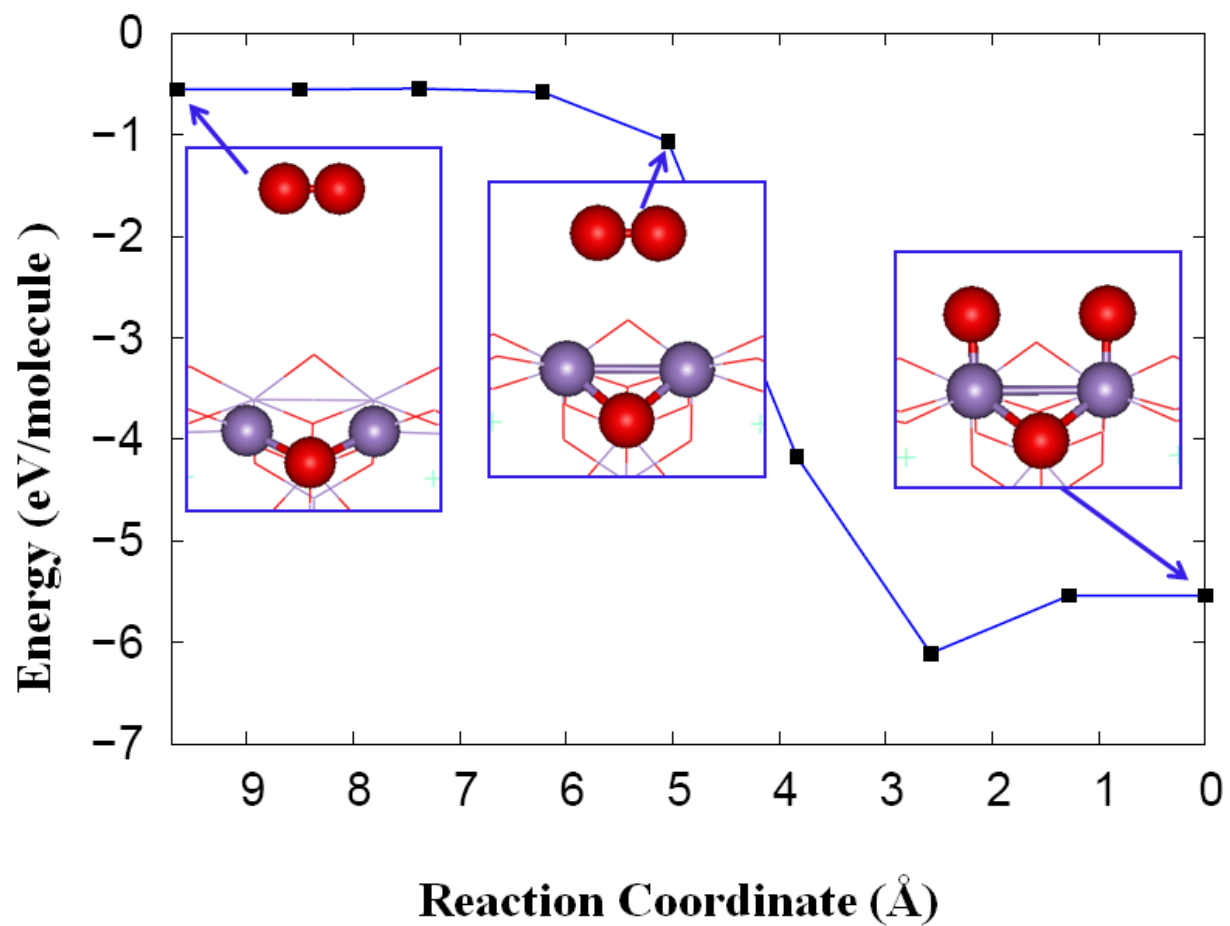


Fig. S4.

NEB reaction route for O₂ dissociation on the Mn-Mn dimer on the stepped SmMn₂O₅ (110) surface. Red and purple balls represent O and Mn, respectively.

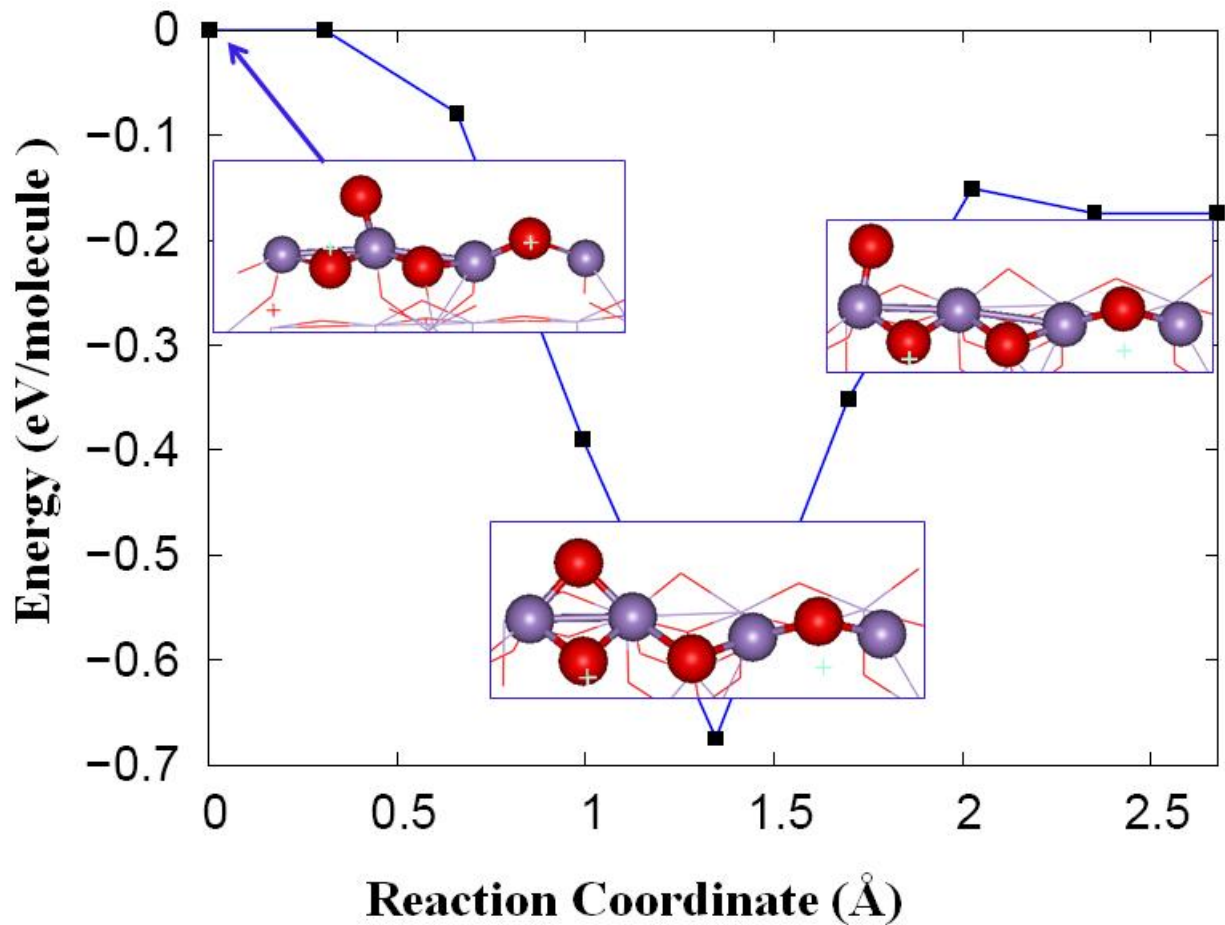


Fig. S5.

Potential energies for atomic O* diffusion on Mn-Mn dimer on the stepped SmMn_2O_5 (110) surface. Red and purple balls represent O and Mn, respectively.

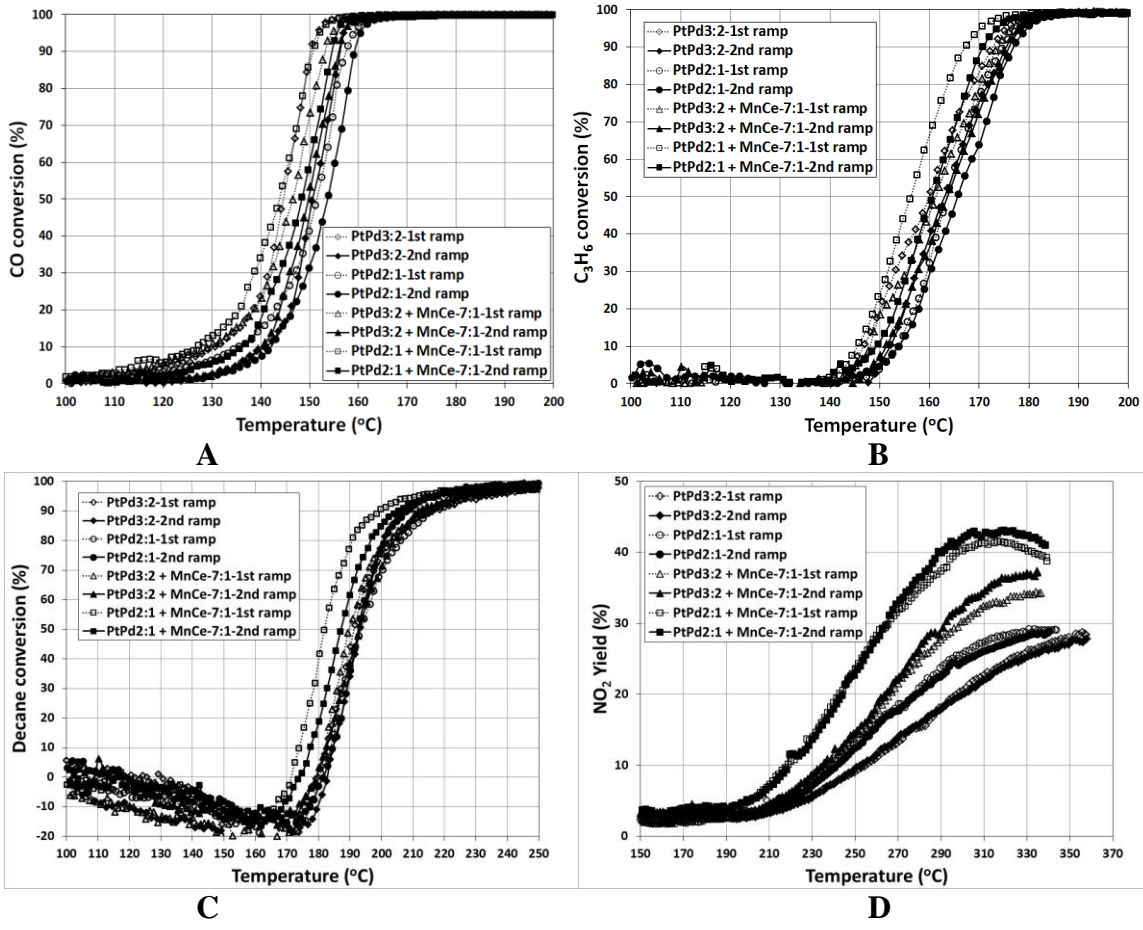


Fig. S6. (A) – (D)

CO, C₃H₆, *n*-decane conversion and NO₂ yield, respectively, as a function of temperature in the core test.

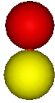
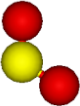
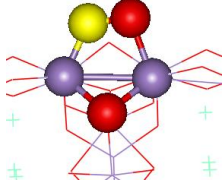
Table S1.

Surface area measurements for hydrothermally aged (10h, 820°C, 10% steam) powders

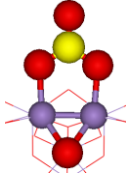
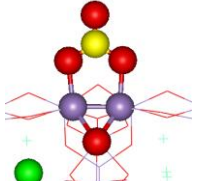
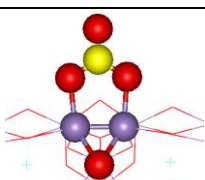
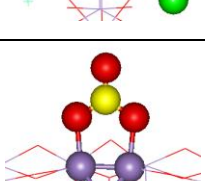
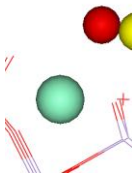
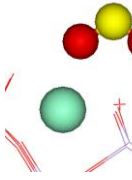
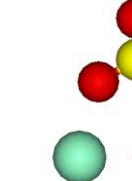
Sample	Surface Area (m ² /g)
Mn ₇ CeSmSrO _{14.83}	25.8
SmMn ₂ O ₅	13.7
Sr _{1.03} MnO _{2.82}	4.9
MnO _x	4.2
CeO ₂	7.6

Table S2.

Calculated and experimental wavenumbers for NO_(g), NO_{2(g)} and NO_x adsorbed species on ideal and stepped SmMn₂O₅ (110) surfaces. Red, purple, green, light green and yellow balls represent O, Mn, Sr, Sm and N, respectively.

		N-O wavenumber (cm ⁻¹)	N-O wavenumber (cm ⁻¹)
NO (g)		1940 [1741–1952 (Ref. 19)]	
NO ₂ (g)		1673 [1628-1654 (Ref. 10)]	
Stepped (110) Surface (Mn-nitrosyl, Mn-NO)			
Mn-NO (clean surface)		1176	617

Mn-NO(clean surface)		1829	555
Mn-NO(clean surface)		1450	406
Mn-NO(clean surface)		1548	509
Stepped (110) Surface (Mn-nitrite, Mn-NO₂)			
Mn-NO ₂ (clean surface)		1850	813
Mn-NO ₂ (Sr-dopant,T1)		1503	728
Mn-NO ₂ (Sr-dopant,T2)		1625	729
Mn-NO ₂ (Sr-dopant,T3)		1592	725
Stepped (110) Surface (Mn-nitrate, Mn-NO₃)			

Mn-NO ₃ (bidentate, clean surface)		1579	1093
Mn-NO ₃ (Sr-dopant,T1)		1604	1058
Mn-NO ₃ (Sr-dopant,T2)		1620	1104
Mn-NO ₃ (Sr-dopant,T3)		1416	1118
Oxidized (110) Surface (Sm, Sm-NO_x)			
Sm-NO (clean surface)		1698	162
Sm-NO ₂ (clean surface)		1311	1151
Sm-NO ₃ (clean surface)		1604	1276

Sm-NO ₃ (clean surface)		1524	1241
Sm-NO ₃ (clean surface)		1523	1248

Table S3.

Core test sample PGM loadings with and without MnCe-7:1

Sample ID	Layers	Targeted Metal Loadings		
		Total PGM g/ft ³	Pt g/ft ³	Pd g/ft ³
PtPd2:1	1	50	33	17
PtPd2:1+ MnCe-7:1	2	50	33	17
PtPd3:2	1	50	30	20
PtPd3:2+ MnCe-7:1	2	50	30	20

References and Notes

1. C. H. Bartholomew, R. J. Farrauto, Fundamentals of industrial catalytic process (Wiley, Hoboken, NJ, ed. 2, 2006).
2. M. A. Tas, R. van Hardeveld, E. M. van Veldhuizen, *Plasma Chem. Plasma Process.* **17**, 371 (1997). [doi:10.1023/A:1021818313047](https://doi.org/10.1023/A:1021818313047)
3. W. Niessen, O. Wolf, R. Schruft, M. Neiger, The influence of ethene on the conversion of in a dielectric barrier discharge. *J. Phys. D* **31**, 542 (1998). [doi:10.1088/0022-3727/31/5/011](https://doi.org/10.1088/0022-3727/31/5/011)
4. P. Schmitz, R. Baird, NO and NO₂ Adsorption on barium oxide: Model study of the trapping stage of NO_x conversion via lean NO_x Traps. *J. Phys. Chem. B* **106**, 4172 (2002). [doi:10.1021/jp0133992](https://doi.org/10.1021/jp0133992)
5. C. H. Kim, G. Qi, K. Dahlberg, W. Li, Strontium-doped perovskites rival platinum catalysts for treating NO_x in simulated diesel exhaust. *Science* **327**, 1624 (2010). [doi:10.1126/science.1184087](https://doi.org/10.1126/science.1184087) [Medline](#)
6. Y. Wen, C. Zhang, H. He, Y. Yu, Y. Teraoka, Catalytic oxidation of nitrogen monoxide over La_{1-x}Ce_xCoO₃ perovskites. *Catal. Today* **126**, 400 (2007). [doi:10.1016/j.cattod.2007.06.032](https://doi.org/10.1016/j.cattod.2007.06.032)
7. P. Patnaik, *Dean's Analytical Chemistry Handbook* (McGraw-Hill, New York, ed. 2, 2004.).
8. S. Brunauer, P. H. Emmett, E. Teller, Adsorption of gases in multimolecular layers. *J. Am. Chem. Soc.* **60**, 309 (1938). [doi:10.1021/ja01269a023](https://doi.org/10.1021/ja01269a023)
9. N. Tang, Y. Liu, H. Wang, Z. Wu, Mechanism study of NO catalytic oxidation over MnO_x/TiO₂ Catalysts. *J. Phys. Chem. C* **115**, 8214 (2011). [doi:10.1021/jp200920z](https://doi.org/10.1021/jp200920z)
10. NIST Chemistry WebBook, <http://webbook.nist.gov/>
11. P. Fornasiero, J. Kaspar, Infrared study of nitric oxide (NO) adsorption and conversion on CeO₂-ZrO₂ mixed oxide. *Collect. Czech. Chem. Commun.* **66**, 1287 (2001). [doi:10.1135/cccc20011287](https://doi.org/10.1135/cccc20011287)
12. S. S. Mulla *et al.*, Reaction of NO and O₂ to NO₂ on Pt: Kinetics and catalyst deactivation. *J. Catal.* **25**, 389 (2006). [doi:10.1016/j.jcat.2006.05.016](https://doi.org/10.1016/j.jcat.2006.05.016)
13. G. A. Tritsarlis, J. Greeley, J. Rossmeisl, J. K. Nørskov, Atomic-scale modeling of particle size effects for the oxygen reduction reaction on Pt. *Catal. Lett.* **141**, 909 (2011). [doi:10.1007/s10562-011-0637-8](https://doi.org/10.1007/s10562-011-0637-8)
14. N. V. Skorodumova, S. I. Simak, B. I. Lundqvist, I. A. Abrikosov, B. Johansson, Quantum origin of the oxygen storage capability of ceria. *Phys. Rev. Lett.* **89**, 166601 (2002). [doi:10.1103/PhysRevLett.89.166601](https://doi.org/10.1103/PhysRevLett.89.166601) [Medline](#)
15. www.crystalimpact.com/pcd/
16. W. Kohn, A. D. Becke, R. G. Parr, Density functional theory of electronic structure. *J. Phys. Chem.* **100**, 12974 (1996). [doi:10.1021/jp960669I](https://doi.org/10.1021/jp960669I)
17. G. Henkelman, H. Jónsson, Improved tangent estimate in the nudged elastic band method for finding minimum energy paths and saddle points. *J. Chem. Phys.* **113**, 9978 (2000). [doi:10.1063/1.1323224](https://doi.org/10.1063/1.1323224)

18. I. Kagomiya, K. Kohn, T. Uchiyama, Structure and ferroelectricity of RMn_2O_5 .
Ferroelectrics **280**, 131 (2002). [doi:10.1080/00150190214799](https://doi.org/10.1080/00150190214799)
19. G. Guelachvili *et al.*, High resolution wavenumber standards for the infrared. *Spectrochim. Acta A Mol. Biomol. Spectrosc.* **52**, 717 (1996). [doi:10.1016/0584-8539\(96\)01717-5](https://doi.org/10.1016/0584-8539(96)01717-5)